Intelligent approach on sensorless control of permanent magnet synchronous generator

International Journal of Power Electronics and Drive System (IJPEDS)
Vol. 13, No. 3, September 2022, pp. 1770∼1778
ISSN: 2088-8694, DOI: 10.11591/ijpeds.v13.i3.pp1770-1778

Intelligent approach on sensorless control of permanent magnet synchronous generator

Subramanian Vijayalakshmi[1], Velappa Ganapathy[2], Chandrasekar Anuradha[1], Raghavan Chandran Ilambirai[1], Viswanathan Ganesh[3]
[1]Department of Electrical and Electronics Engineering, SRM Institute of Science and Technology, Tamil Nadu, India
[2]Department of Information Technology, SRM Institute of Science and Technology, Tamil Nadu, India
[3]Department of Energy and Environment, Chalmers University of Technology, Gothenburg, Sweden

Article Info

Article history:

Received May 12, 2022
Revised Jun 12, 2022
Accepted Jun 29, 2022

Keywords:

Feed forward neural network
Maximum power point
Permanent magnet synchronous generator
Sliding mode control

ABSTRACT

In this paper, a standalone permanent magnet synchronous generator (PMSG) system is designed to generate power at maximum power point (MPP). The variable speed operation of wind energy conversion system consists of PMSG, controlled rectifier and voltage source inverter co to the load. Proportional integral (PI), sliding mode (SM), and feed forward neural network (FFNN) control strategies are applied in field oriented control (FOC) at generator side converter. A comparative study on power generated at maximum power point (MPP) is done with these controllers using simulation. Hill climb search (HCS) method is applied to attain MPP. Load side inverter control strategy involves the PI and SM controllers in order to maintain the unity power factor and to control the active and reactive power for nonlinear load. The control strategies are modelled and simulated with MATLAB/Simulink. The effectiveness of proposed control method is demonstrated using simulation results.

Corresponding Author:

Subramanian Vijayalakshmi
Department of Electrical and Electronics Engineering, SRM Institute of Science and Technology
Chennai, Tamil Nadu, India
Email: vijis_india@yahoo.co.in

1. INTRODUCTION

The attractiveness of employing renewable energy sources rises as the need for power grows and global warming intensifies. Because they are direct driven devices, permanent magnet synchronous generator (PMSGs) are frequently used for variable speed operation. As a result, PMSGs are designed to extract the greatest power from the wind. A supervisory control is built [1] to accomplish efficient functioning of the wind energy conversion system (WECS), and control methods are employed to reduce losses in the generator. The zero-direct axis current (ZDC) control technique is utilized to decrease windage losses in the generator [2]. To reduce resistive loss in induction generators, a minimum ohmic loss (MOL) technique is provided. maximum power point (MPP) tracking and MOL control are handled by the fuzzy logic controller (FLC). Experiment findings verified the effectiveness of the control approach [3].

The WECS includes a shunt active power filter (SAPF) to counteract harmonic currents. To compensate for harmonic currents, the SAPF generates compensatory currents that have the same magnitude as the harmonic currents but are phase opposite. On the grid-side, the SAPF reduces distorted current. This remote wind farm's generator's rotational speed can be precisely controlled by creating a new electrical PMSG using finite element method simulations (FEM). A neodymic iron boron radial flux generator is designed for PMSG

low-speed spinning [5]. A nonlinear control method is used to generate MPP. The nonlinear controller used to improve the system's dynamic performance is built using average theory and Lyapunor stability [6]. PMSG output power and rotor speed characteristics can now be analyzed in an entirely new way. To make WECS management simple, wind turbine electrical design characteristics such as losses and power output are kept to a minimum. Due to the fast-changing wind speed, the DFIG's performance can be improved with FLC in the rotor and grid side converters. MATLAB/Simulink [8] is used for the control operation. It's possible to measure the dynamic field induced by the doubly-fed induction generator (DFIG) under various operating conditions with power systems computer aided design (PSCAD) and the electromagnetic transient program (EMTP). Also shown is a third-order DFIG model. With the help of grid codes, the WECS can be operated using the fault ride through (FRT) control. An MPP algorithm comparison is carried out [9]. The simpower system in MATLAB is used to simulate the various control algorithms in order to evaluate their efficacy and dynamics. Higher MPP extraction performance was achieved with sensorless FLC controls [10]. Lower order harmonics are reduced on the grid side [11]. A proportional-integral (PI) controller and an LCL filter are used to improve power quality [12], [13]. PI, fuzzy, and artificial neural network (ANN) are used in tandem to achieve appropriate system control performance. The PI controller, which focuses on pitch angle control, is compared with optimization strategies to achieve the goal [14], [15]. Babu and Arulmozhivarman [16] talks about the evaluations of MPPT methods. Research in this area examines the performance of a WECS that is controlled by FOC at the generator side converter and VOC at the load side converter. A back-to-back PWM converter is connected to the load [17], [18]. You can monitor the generator's actual rotational speed by using the model reference adaptive system. When the wind speed changes, the generator side converter controller at MPP speeds up the generator to deliver the most power possible [19], [20]. The PI, sliding mode controller (SMC), and feed-forward neural network (FFNN) controllers are used in the flux oriented control (FOC) speed control loop. SMC and PI are used to control the load side converter's DC-link voltage, active power, and reactive power. As a result of this, the power factor does not change. MATLAB's Simulink is used to verify the results.

2. WIND TURBINE GENERATOR

The wind turbine converts the available wind into mechanical power which makes the generator to rotate. The mechanical wind turbine power could be expressed by (1).

$$P_m = \frac{1}{2}\pi r^2 C_p(\lambda, \beta) V^3 \tag{1}$$

Where ρ is the density of air in Kg/m^3, r is the radius of the blade (m), C_p is the turbine performance coefficient which is the function of tip speed ratio (λ) and the blade pitch angle (β). The is expressed as (2) where r is the turbine rotor speed (rad/sec) and V is the velocity of the wind (m^2) respectively.

$$\lambda = \frac{\omega_m r}{V} \tag{2}$$

2.1. Permanent magnet synchronous generator

The equations governing the model of PMSG in the rotating reference frame are given by the equations (3) and (4) [21].

$$\frac{di_{qs}}{dt} = \frac{1}{L_q}[v_{qs} - R_s i_{qs} - \omega_e L_d i_{ds} - \omega_e \phi_f] \tag{3}$$

$$\frac{di_{ds}}{dt} = \frac{1}{L_d}[v_{ds} - R_s i_{ds} + \omega_e L_q i_{qs}] \tag{4}$$

Where v_{qs} and v_{ds} are the stator d and q axes voltage, i_{qs} and i_{ds} are the stator d and q axes currents, L_d and L_q are the stator inductances, ϕ_f is the rotor permanent magnet flux. ω_e is the electrical rotational speed of the generator given by (5).

$$\omega_e = p\omega_m \tag{5}$$

Where p is the number of pole pairs and ω_m is the mechanical rotational speed of the generator. Assuming a non-salient pole PMSG the d and q axes inductances will be equal. The resulting torque equation T_e is given by (6).

$$T_e = \frac{3}{2} p \phi_f i_{qs} \tag{6}$$

2.2. MPP control strategy

Since the blade radius and air density are constants, the power collected by the turbine equals Cp. Operating the turbine at the optimal tip speed ratio maximizes the Cp value. A wind turbine's maximum power is obtained by regulating the generator's rotor speed to achieve an ideal tip speed ratio. The equation determines the turbine's maximum mechanical power given by (7).

$$P_{max} = \frac{1}{2} \rho a C_{pmax} (\frac{r \omega_{opt}}{\lambda_{opt}})^3 \tag{7}$$

Where a is the area of the turbine, ω_{opt} is the optimum speed of the turbine, λ_{opt} optimum tip speed ratio. To generate the optimum speed for maximum power extraction a HCS algorithm is introduced which requires only wind speed as the input.

3. GENERATOR SIDE CONVERTER CONTROL

As indicated in Figure 1 of the WECS, FOC is applied at the generator side converter. The rotor speed controls the electromagnetic torque in FOC control. FOC needs rotor position and generator speed to regulate. Model reference adaptive system (MRAS) determines rotor position and speed. The generator's stator current regulates the generator's torque. So the torque is dictated by the stator current's q-axis component [22], [23]. FOC has two loops: speed and current. PMSG is compared to the MPPT algorithm's reference speed. MRAS calculates the generator's true speed. The speed controller outputs the q-axis reference current i_q^*. The generator side converter control scheme is shown in Figure 1. We use a standard HCS approach to optimize MPPT speed. The FOC speed control loop uses PI, SMC, and FFNN control algorithms. Section 5 describes the results of simulating the controllers in MATLAB Simulink.

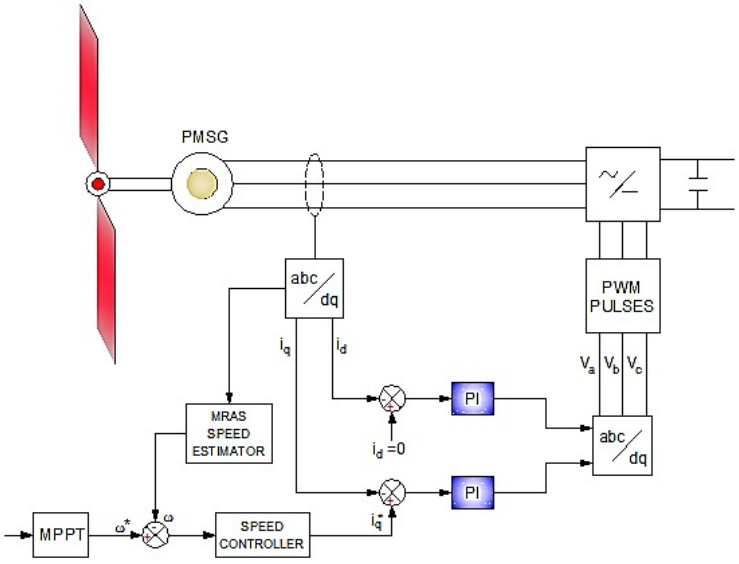

Figure 1. Block diagram of proposed wind energy conversion system

3.1. Sliding mode control

In the speed controller, a nonlinear SMC is used to keep the generator speed at the optimal speed for extracting maximum power. FOC features a current loop inside and a speed loop outside. A SMC controls the speed loop, while two PI controllers regulate the current loop. The SMC's first step is to sketch the sliding surface. The speed regulator's sliding surface is provided by (8). Differentiating (8) with respect to time and after simplification the control (9) for i_q^* is obtained.

$$S_w = \omega_{opt} - \omega_{est} \tag{8}$$

$$i_q = \frac{2}{3p\phi_f}[T_m + F\omega_{est} + J\frac{d\omega_{opt}}{dt} + JKsgn(S_\omega)] \tag{9}$$

3.2. Feed forward neural network

The network is made up of three layers: one input layer, one hidden layer, and an output layer. In the output layer, a linear activation function is utilized. The network is trained using the Levenberg-Marquardt algorithm [24]. The speed and current of the training data are obtained through simulation without the need of a controller. The FFNN controller receives the optimal and estimated speed from MRAS as error input. The reference current is generated by the FFNN controller. The reference currents on the d and q axes are compared to the actual currents using a PI controller. The rectifier receives pulse width modulation (PWM) pulses. The generator speed is changed by controlling the rectifier appropriately in order to obtain the most power out of the turbine. X is the input training vector which is speed and Y is the output which is current. x_i is the input neuron which is speed and $y_k$is the output neuron which is the quadrature axis current and Z_{inj} is the hidden layer represented in the Figure 2 is the connection weight of the input layer. Z_j is the output signal and is and is the function of hidden layer Z_{inj} is given by (10). w_{ok} is the bias of output unit and w_{jk} is the connection weight of the output layer. The output signal is as (11).

$$Z_j = f(Z_{inj}) \tag{10}$$

$$y_k = f(w_{ok} + \sum_j z_j w_{jk}) \tag{11}$$

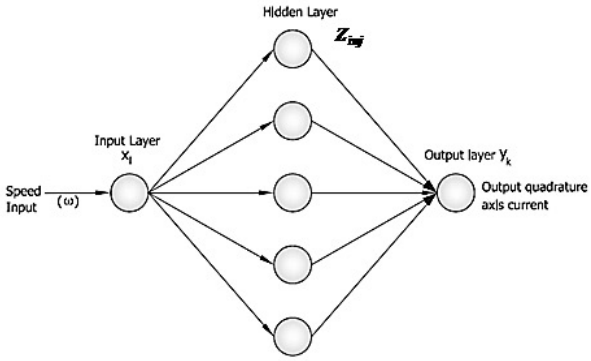

Figure 2. FFNN-architecture

4. CONTROL OF LOAD SIDE CONVERTER

For the most part, load side controllers are used to control the output voltage and frequency. The active and reactive powers of the load can be adjusted with its help. Changeable structure SMC is used as a load controller in this article. Two loops dominate the DC Link voltage and current control architecture. A PI controller is used to keep the DC Link voltage constant. Two current loops are controlled by SMC. The load-side inverter is controlled by vector control. Two loops are used for control, The inner loop controls the direct and quadrature currents. DC link voltage is maintained at a predetermined level by the second loop. Using a phase locked loop (PLL), the load voltage phase angle can be detected and recorded. Figure 3 shows the block diagram of the converter's load side. The equations for the load-side converter voltages in the synchronously rotating reference given by (12) and (13).

$$V_{gd} = V_d - R_f i_{gd} - L_f \frac{di_{gd}}{dt} + \omega L_f i_{gd} \tag{12}$$

$$V_{gq} = V_q - R_f i_{gq} - L_f \frac{di_{gq}}{dt} - \omega L_f i_{gq} \tag{13}$$

Where V_{gd} and V_{gq} are d q-axes load voltages. i_{gd} and i_{gq} are d-axis and q-axis load currents. R_f -Filter Resistance, L_f - Filter Inductance. Vector control strategy is depending on a synchronously rotating reference frame. Active power P and reactive power Q are expressed as $P = \frac{3}{2} V_d i_{gd}$ and $Q = \frac{3}{2} V_d i_{gq}$.

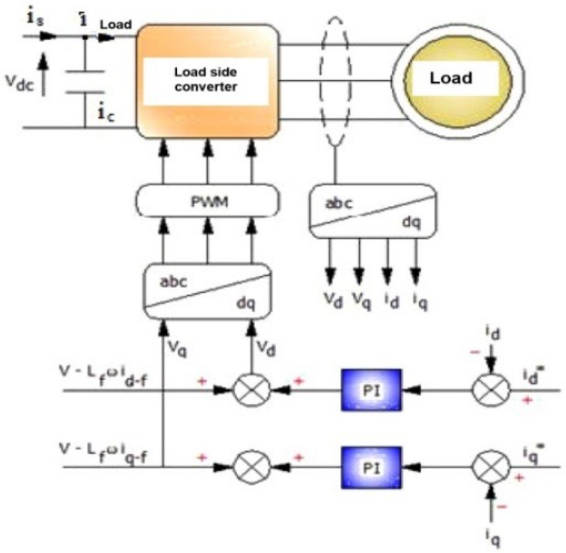

Figure 3. Load side converter–block diagram

As a result, d-q-axes current may govern both active and reactive powers. There are two control loops in the system. The SMC [25] is used in the inner loop that regulates the load side current. The DC Voltage control is attached to the outside loop. The DC voltage controller generates the reference current for the d-axis current in order to manage the active power. The reference value for reactive power is set to zero. Sliding surfaces are introduced as (14) and (15).

$$S_{df} = i_{drf} - i_{df} \tag{14}$$

$$S_{qf} = i_{qrf} - i_{qf} \tag{15}$$

Where i_{drf}, and i_{qrf} are the desired values of d- q-axes currents respectively. As the sliding mode occurs on the sliding mode control surface, then differentiating equation (14)and (15) with respect to dt and equal to zero. Simplifying the control voltages of dq axes given by (16) and (17).

$$V_{drf} = L_f \frac{di_{drf}}{dt} + R_f i_{df} - L_f \omega i\_qf + V + k_{df} sgn(S_{df}) \tag{16}$$

$$V_{qff} = R_f \frac{di_{qf}}{dt} + L_f \omega i_{df} + k_{qf} sgn(S_{qf}) \tag{17}$$

5. RESULT ANALYSIS

The performance of the HCS method is studied using Simulink in MATLAB. A rectangular type of wind speed is applied to the WECS as illustrated in Figure 4. With HCS method the power coefficient optimum value 0.44 is reached and is maintained at the same value for a wider range of speeds which is shown in Figure 5. Comparative studies on the performances of WECS are carried out between PI, SMC, and FFNN for a wind speed 10 m/s in all the three cases. The reference electrical power is 3200 watts.

The generated electrical powers from, PI, SMC, and FFNN controllers are given in Table 1. From Figure 6 it is seen that the neural controller attains the reference power at 0.14 sec. The power generated using the SMC is 3000 watts which is below the reference value with the settling time of 0.26 sec. The power generated from the PI is 2980 watts with the settling time of 0.26 sec., which is below the reference value. When the FFNN controller is used, the PMSG's power output is found to be at its rated value. Many controllers' electrical power waveforms are shown in the Figure 6. When wind speeds reach 10 m/s, WECS handles a nonlinear load. Load side converters are used to address the simulation results for the PI and SMC controller models The nonlinear load is a balanced active load of 200 ohms connected to a three-phase diode rectifier. The DC link voltage is maintained at 500 V by the load side controller, as shown in Figure 7.

Table 1. Comparison of different controllers

Controller	Reference power (W)	Power generated (W)	% Error in power generated	Settling time (Sec)
ANN	3200	3192	1.02	0.14
SMC		3000	8.6	0.26
PI		2980	9.2	0.2

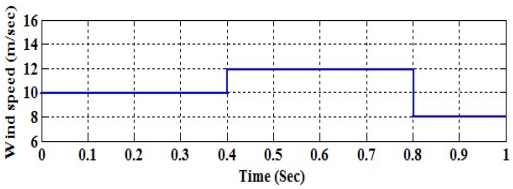

Figure 4. Wind speed (m/sec)

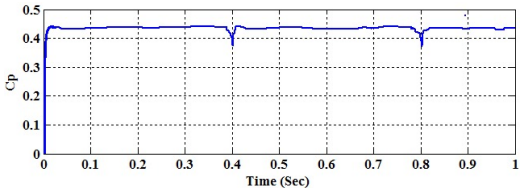

Figure 5. Cp (power coefficient)

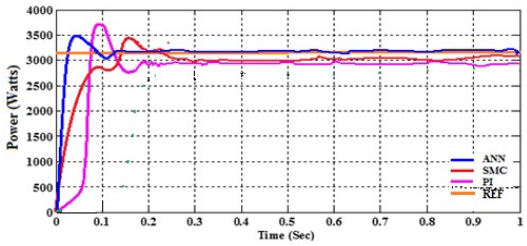

Figure 6. PMSG power for different controllers (W)

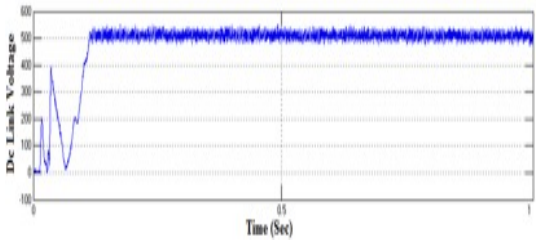

Figure 7. DC link voltage (volts)

MATLAB/Simulink is used to examine the sliding mode technique for load–side converters. The output voltage across the load is depicted in Figure 8. Figures 9 and 10 illustrate the active and reactive powers across the load. The reactive power is controlled to zero by the load side inverter, as shown in Figure 8. It is also clear from Figure 11 that the suggested SMC controller achieves the unity power factor. A comparison of the PI controller's single-phase output voltage and current to the SM controller's load output voltage and current is

shown in Figure 12. Sliding Mode Controller load currents and total harmonic distortion (THD) outputs from the PI controller are shown in Figures 13 and 15. Figure 13 shows the relationship between voltage and current in terms of phase. As a result, the power factor of the SM controller is equal to one. Using the fast fourier transform (FFT), it is possible to determine the harmonic content of the nonlinear load's current. A nonlinear load on the load side converter is shown in Table 2 percent THD. The proposed SMC has a THD of around 4.02%, which is acceptable, and the results show that the nonlinear control at the load side converter is more effective.

Table 2. %THD of the non-linear load current

Control Type	% THD
PI	17.63
SMC	4.02

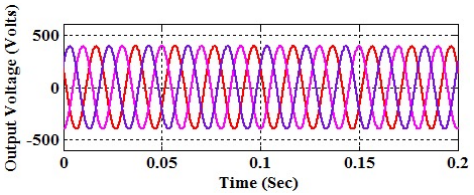

Figure 8. Output voltage across load

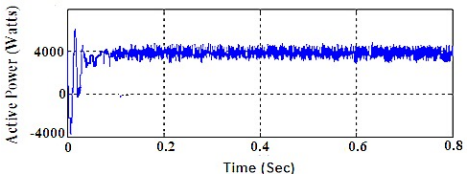

Figure 9. Active power in watts

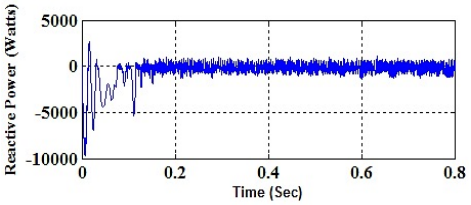

Figure 10. Reactive power in watts

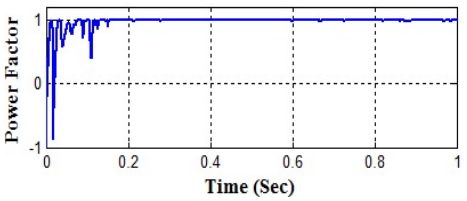

Figure 11. Power factor

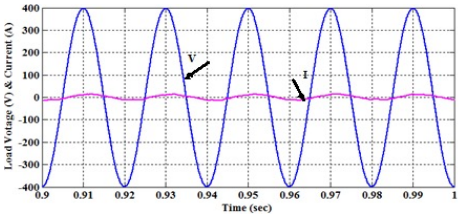

Figure 12. Load voltage (V) and current (A) - PI

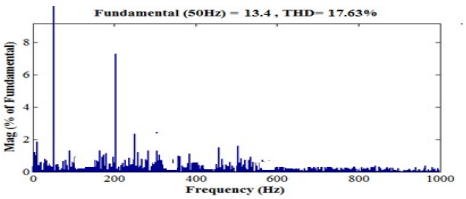

Figure 13. THD of line current at load side-PI

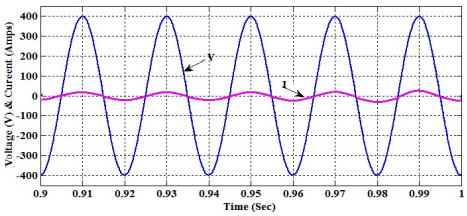

Figure 14. Single phase load voltage (V) and current (A)-SM controller

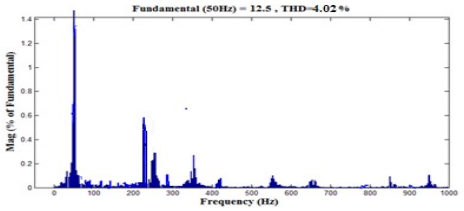

Figure 15. THD analysis of line current at load side-SM controller

6. CONCLUSION

To control the FOC at the generator side of the WECS, the PI, SMC, and FFNN control loops are used in this paper. Simulink in MATLAB is used for the simulation study. When subjected to varying wind speeds, a simulation proved the HCS method's efficacy by maintaining the power coefficient at its optimal level of 0.44. The FFNN controller generates more power than the PI and SM controllers, and it is closer to the reference value. VOC with PI and SM controllers are used to control the load converter. The DC link voltage is kept constant at 500 V. Load current THD factor is 4.02 in SM control, maintaining unity power factor. For nonlinear loads, the SM control proved the ability to control output power with unity power factor.

REFERENCES

[1] Devashish, A. Thakur, S. Panigrahi, and R. R. Behera, "A review on wind energy conversion system and enabling technology," *2016 International Conference on Electrical Power and Energy Systems (ICEPES)*, 2016, pp. 527-532, doi: 10.1109/ICEPES.2016.7915985.

[2] K. Bunjongjit and Y. Kumsuwan, "Performance enhancement of PMSG systems with control of generator-side converter using d-axis stator current controller," *2013 10th International Conference on Electrical Engineering/Electronics, Computer, Telecommunications and Information Technology*, 2013, pp. 1-5, doi: 10.1109/ECTICon.2013.6559492.

[3] A. Mesemanolis, C. Mademlis, and I. Kioskeridis, "High-Efficiency Control for a Wind Energy Conversion System With Induction Generator," in *IEEE Transactions on Energy Conversion*, vol. 27, no. 4, pp. 958-967, Dec. 2012, doi: 10.1109/TEC.2012.2213602.

[4] Z. Wu, X. Dou, J. Chu, and M. Hu, "Operation and control of a direct driven PMSG based wind turbine system with an auxiliary parallel grid-side converter," *Energies*, vol. 6, no. 7, pp. 3405-3421, Jul. 2013, doi: 10.3390/en6073405.

[5] M. Irfan *et al.*, "A design of electrical permanent magnet generator for rural area wind power plant," *International journal of power electronics and drive system*, vol. 9, No. 1, pp. 269-275, Mar. 2018.

[6] Y. Boussairi, A. Abouloifa, I. Lochkar, A. Hamdoun, and C. Aouadi, "Modeling and non linear control of a wind turbine system based on a permanent magnet synchronous generator connected to the three-phase network," *International journal of power electronics and drive system (IJPEDS)*, vol. 9, No. 2, pp. 766-774, Jun. 2018, doi: 10.11591/ijpeds.v9.i2.pp766-774.

[7] A.Verd, O. Lastres, G. Hernaindez, L. Verea, and P. J. Sebestian, "A new method for characterization of small capacity wind turbines with permanent magnet synchronous generator: an experimental study, *Heliyon*, vol. 4, no. 8, Aug. 2018, doi: 10.1016/j.heliyon.2018.e00732.

[8] A. Dida and D. Ben Attous, "Doubly-fed induction generator drive based WECS using fuzzy logic controller," *Frontiers in Energy*, vol. 9, pp. 272-281, 2015, doi: 10.1007/s11708-015-0363-9.

[9] J. Mwaniki, H. Lin, and Z. Dai, "A condensed introduction to the doubly fed induction generator wind energy conversion systems," *Journal of Engineering*, vol. 2017, Jun. 2017, doi: 10.1155/2017/2918281.

[10] K. Belmokhtar, H. Ibrahim, and M. L. Doumbia, "A maximum power point tracking control algorithms for a PMSG based WECS for isolated applications : critical review," in *Wind turbines-Design, control and applications*, pp. 199-209, 2016, doi: 10.5772/63803.

[11] V. Prasath, S. Vijayalakshmi, and R. Jain Anush, "PMSG Based WECS with PR control strategy for grid control," *Applied Mechanics and Materials*, vol. 573, pp 267–272, 2014, doi: 10.4028/www.scientific.net/AMM.573.267.

[12] B. Antar, B. Hassen, B. Babes, and H. Afghoul, "Fractional order PI controller for grid connected wind energy conversion system," *2015 4th International Conference on Electrical Engineering (ICEE)*, 2015, pp. 1-6, doi: 10.1109/INTEE.2015.7416692.

[13] B. Jain, S. Singh, S. Jain, and R. K. Nema, "Flexible mode control of grid connected wind energy conversion system using wavelet," *Journal of Energy*, 2015, doi: 10.1155/2015/152898.

[14] S. Behera, B. Subudhi, and B. B. Pati, "Design of PI controller in pitch control of wind turbine: a comparison of PSO and PS algorithm," *International Journal of Renewable Energy Research-IJRER*, vol. 6, no. 1, pp 271-281, 2016, doi: 10.20508/ijrer.v6i1.3137.g6783.

[15] F. Zhou and J. Liu, "Pitch controller design of wind turbine based on nonlinear PI/PD control," *Shock and Vibration*, vol. 2018, 2018, doi: 10.1155/2018/7859510.

[16] N. R. Babu and P. Arulmozhivarman, "Wind energy conversion systems-a technical review," *Journal of Engineering Science and Technology*, vol. 8, no. 4, pp 493-507, 2013.

[17] S. K. Bhuyan, P. K. Hota, and B. Panda, "Power quality analysis of a grid-connected solar/wind/hydrogen energy hybrid generation system," *International journal of power electronics and drive system (IJPEDS)*, vol. 9, no. 1, pp. 377-389, 2018, doi: 10.11591/ijpeds.v9n1.pp377-389.

[18] T. R. S. de Ereitas, P. J. M. Menegaz, and D. S. L. Simonetti, "Rectifier topologies for permanent magnet synchronous generator on wind energy conversion system: a review," *Renewable and Sustainable Energy Reviews*, vol. 54, pp. 1334-1344, 2016, doi: 10.1016/j.rser.2015.10.112.

[19] M. Nasiri, J. Milimonfared, and S.H. Fathi, "Modeling, analysis and comparison of TSR and OTC methods for MPPT and power smoothing in permanent magnet synchronous generator based wind turbines," *Energy Conversion and Management*, vol. 86, pp. 892-900, 2014, doi: 10.1016/j.enconman.2014.06.055.

[20] S. Vijayalakshmi, C. Anuradha, E. Kovendan, and V. Rattankumar, "Performance of wind energy conversion system using a permanent magnet synchronous generator for maximum power point tracking," *2012 International Conference on Emerging Trends in Electrical Engineering and Energy Management (ICETEEEM)*, 2012, pp. 417-421, doi: 10.1109/ICETEEEM.2012.6494482.

[21] S. Ezhilarasan, V. Ananthapadmanabhan, and P. Avirajamanjula, "Control scheme for a stand-alone wind energy conversion system for better efficiency of battery storage," *International Journal of Applied Engineering Research*, vol.13, no. 19, pp 14359-14364, 2018.

[22] F. E. Tahiri, K. Chikh, and M. Khafallah, "MPPT strategy using fuzzy-PI controller applied to a standalone wind energy conversion system," *SCA '18: Proceedings of the 3rd International Conference on Smart City Applications*, 2018, pp 1-7, doi: 10.1145/3286606.3286847.

[23] U. S. Anjaneyulu, B. S. Rao, and P. G. Naidu, "Control of PMSG wind turbine based on PI/ANN controllers under unbalanced grid voltage and nonlinear load conditions," *International Journal of Electrical and Computer Engineering*, vol. 8, no. 2, pp. 153-166, 2016.
[24] Q. Wang and L. Chang, "An intelligent maximum power extraction algorithm for inverter-based variable speed wind turbine systems," in *IEEE Transactions on Power Electronics*, vol. 19, no. 5, pp. 1242-1249, Sep. 2004, doi: 10.1109/TPEL.2004.833459.
[25] S. Ciampichetti, M. L. Corradini, G. Ippoliti, and G. Orlando, "Sliding mode control of permanent magnet synchronous generators for wind turbines," *IECON 2011 - 37th Annual Conference of the IEEE Industrial Electronics Society*, 2011, pp. 740-745, doi: 10.1109/IECON.2011.6119402.

BIOGRAPHIES OF AUTHORS

Subramanian Vijayalakshmi in 2006, she earned a Bachelor of Engineering degree in Electrical and Electronics Engineering from Madras University and a Master of Engineering degree in Power Electronics and Industrial Drives. She is presently an Assistant Professor at the SRM Institute of Science and Technology's Department of Electrical and Electronics Engineering in Chennai, India. She holds a Ph.D. in wind energy conversion systems. Her interests include power electronics and renewable energy systems. She has papers published in a number of prestigious magazines. She can be contacted at email: vijis_india@yahoo.co.in.

Velappa Ganapathy received his B.E. from Government College of Technology, Coimbatore, and his MSc (Engg.) from P.S.G. College of Technology, Coimbatore. He received his PhD from IIT Madras in 1982. Velappa Ganapathy is an Information Technology Professor at SRM Institute of Science and Technology. From 1964 to 1997, he taught at the Government College of Technology in Coimbatore and the Anna University in Chennai. Until July 2013, he worked at Multimedia University, Cyberjaya, Monash University, Sunway Campus, and University of Malaya in Kuala Lumpur. His research interests include DSP, soft computing, power system analysis, neural networks, fuzzy logic, genetic algorithms, robotic navigation, bond graph, VLSI design, image processing, computer vision, and SOA. He has 60 publications in international journals and 110 in international conference proceedings. He can be contacted at email: ganapatv@srmist.edu.in.

Chandrasekar Anuradha Madras University awarded her a Bachelor of Engineering Degree in Electrical and Electronics Engineering in 2004 and a Master of Engineering Degree in Power Electronics and Drives in 2010. She is presently an Assistant Professor at the SRM Institute of Science and Technology's Department of Electrical and Electronics Engineering in Chennai, India. She earned a Ph.D. in Multiport DC-DC converters. Her interests include power electronics and renewable energy systems. She can be contacted at email: anuradhc@srmist.edu.in.

Raghavan Chandran Ilambirai Madras University awarded her a Bachelor of Engineering Degree in Electrical and Electronics Engineering in 2002 and a Master of Engineering Degree in Power Electronics and Drives in 2004. She is presently an Assistant Professor at the SRM Institute of Science and Technology's Department of Electrical and Electronics Engineering in Chennai, India. She earned her Ph.D. in the field of Zeta DC-DC converters. She can be contacted at email: ilambirr@srmist.edu.in.

Viswanathan Ganesh received his bachelor's degree in Electrical and Electronics Engineering from SRM Institute of Science and Technology in 2021, currently he is pursing master's degree in sustainable Electric Power Engineering and Electromobility from Chalmers University of Technology. His research areas include electric vehicles, renewable energy integration, and power system analysis. He can be contacted at email: ganeshvi@student.chalmers.se.